Building Tomorrow's Society
*Bâtir la Société de Demain*

Fredericton, Canada
June 13 – June 16, 2018/ *Juin 13 – Juin 16, 2018*

# A COMPARISON OF RECENTLY DEVELOPED ANALYTICAL MODELS FOR STEEL MOMENT-RESISTING FRAME CONNECTIONS

Steneker, Paul[1, 5], Wiebe, Lydell[2] and Filiatrault, Andre[3, 4]
[1] Graduate Student, McMaster University, Canada
[2] Assistant Professor, McMaster University, Canada
[3] Professor, University at Buffalo State University of New York, USA
[4] Professor, University School for Advanced Studies IUSS, Italy
[5] stenekpr@mcmaster.ca

**Abstract:** The investigations following the unacceptable performance of moment resisting frames (MRF) in steel structures during the 1994 Northridge Earthquake identified issues in the weld detailing of the connections used. These original MRF connections, commonly known as pre-Northridge connections, have been identified as having a less ductile performance than anticipated. Research efforts immediately following the Northridge earthquake have resulted in the development of a variety of connections that are identified as pre-qualified, allowing these connections to be selected by designers for implementation without the need for component-level validation. Further research has been conducted to develop other alternate connections. Some of this research has resulted in a series of MRF connections that have been developed to allow for full hysteretic behaviour without the resulting damage due to plastic hinging of the beam. Connections such as the sliding hinge joint (SHJ) dissipate large amounts of energy through friction rather than plastic yielding. Modifications to these connections have resulted in a SHJ connection with self centering behaviour (SCSHJ). This paper examines the specific behaviour of some of the available moment resisting connections and the calibration of the analytical tools used to model each connection. A summary of the hysteretic performance of each connection is presented and a comparison is conducted between the hysteretic behaviours of pre-Northridge, several pre-qualified connections and newly developed low-damage connections such as the SHJ and SCSHJ connections. Analytical models are developed for each type of connection in OpenSees based upon the available component test data. The calibration of these models is discussed and the resulting parameters are summarized to enable both researchers and designers to implement these connection models in future frame analyses. Finally, the collapse analysis of a case-study frame incorporating these various MRF connections is presented.

## 1 INTRODUCTION

The Northridge Earthquake had far reaching impacts on the design of steel moment resisting frames (MRF) in seismic areas (Bruneau et al. 2011). The resulting investigation highlighted the poor performance of the beam-to-column connections, due to fractures in and around the welds connecting the beam flanges to the column (FEMA-350 2000). To address these problems with pre-Northridge connections, the SAC research program developed seven prequalified connections that have demonstrated adequate performance during cyclic component testing. Such connections are currently approved for use in seismic areas of Canada and the United States without further investigation (CISC 2014, AISC 2016). Other research efforts have focused on the development of high-performing MRF connections that use mechanical devices rather than plastic yielding as an energy dissipation method (Khoo et al. 2013). This research has been conducted over

the last decade and involved several iterations of hinging connections, referred to as Sliding Hinge Joint (SHJ) and its self centering variant (SCSHJ).

This paper examines the hysteretic behaviour of seven beam-to-column moment resisting connections. The specific hysteretic characteristics of each connection are discussed, and an analytical model is proposed for each connection in OpenSees (McKenna & Scott 2000). This includes two newly developed analytical models for the SHJ and SCSHJ connections, which are presented in detail. The collapse performance of an identical frame modelled with the seven different connections is presented. Furthermore, a sensitivity analysis is used to quantify the impact on the frame collapse performance when using alternative methods to capture the reloading stiffness behaviour of beam hinge connections.

## 2 HYSTERETIC MODELS

Seven hysteretic beam hinge models were calibrated within the scope of this study. These calibrations were conducted using available component test data, a majority of which was obtained using the online database provided by Lignos and Al-Shawwa (2010). The analytical models were calibrated in OpenSees using existing material models. Each connection has its own hysteretic characteristics, sometimes requiring multiple material models to be combined to achieve the desired calibration.

Figure 1(a) demonstrates the component test results for a typical pre-Northridge (PRENORTH) connection (Engelhardt and Sabol 1994). This connection experiences early strength deterioration, occurring at approximately 0.01 rad, when compared to the other six connections (shown in Fig. 1(b) to (g)), which maintain positive post yield strength increase up to approximately 0.02 rad. The reduced beam section (RBS), shown in Figure 1 (b) (Popov et al. 1998), has the lowest yield moment of the first five “classic” MRF connections, which is a direct result of the cuts made in the beam flanges. The welded unreinforced flange (WUF) connection is similar in assembly process to the PRENORTH, with the major difference being the welding detailing, which includes specific weld hole geometry and removal of the backing bar (CISC 2014). These details appear to have a positive impact as experimental component tests, shown in Figure 1 (c) (Choi et al. 2002), demonstrate ductile behaviour up to 0.05 rad of rotation. The welded unstiffened end plate (WUEP) connection, whose test results are shown in Figure 1 (d) (Sumner & Murray 2002), has a unique pinching behaviour when compared to the other five “classic” MRF connections. This is mainly due to the prying of the end plate and bolts. Furthermore, this connection appears to have less strength capability at large rotations. In contrast, the welded stiffened end plate (WSEP) connection does not have the same pinching behaviour than its unstiffened counterpart, as shown in Figure 1 (e) (Sumner & Murray 2002). As a result of the added stiffeners, this connection has an increased yield moment and a smaller strength deterioration at large deformations.

Figure 1 (f) and (g) illustrate the experimental component test results of the newly developed sliding hinge joint (SHJ) and self centering sliding hinge joint (SCSHJ) connections, respectively (Khoo et al. 2013). Since these assemblies are designed to have an activation moment that must always be lower than the yield moment of the beam, the results of the component tests and subsequent analytical models were normalized by the yield moment of the beam section used for the test and not the activation force of the connection assembly. This facilitates comparison of the normalized moment values across the seven connections. In contrast to the first five “classic” connections, the SHJ connection has increasing levels of energy dissipation per cycle as the deformations are increased. This unique behaviour stems from the use of friction as an energy dissipation mechanism rather than plastic deformation. The SHJ connection has three distinct stiffness portions in its backbone curve, corresponding to stages of the deformation sequence of this connection. These various stiffness values can be modified to achieve the designer’s desired behaviour as several of the connections components can be selected independently (Khoo et al. 2013). While the SCSHJ connection shares many of the same characteristics of the SHJ connection, the addition of a ring spring assembly in the connection results in a flag shaped hysteresis loop. The same adjustability of the connection behaviour that is available in the SHJ connection is also available in the SCSHJ connection, with the addition of the relative degree of self-centering behaviour, which can also be selected by the designer simply by using a different ring spring assembly (Khoo et al. 2013).

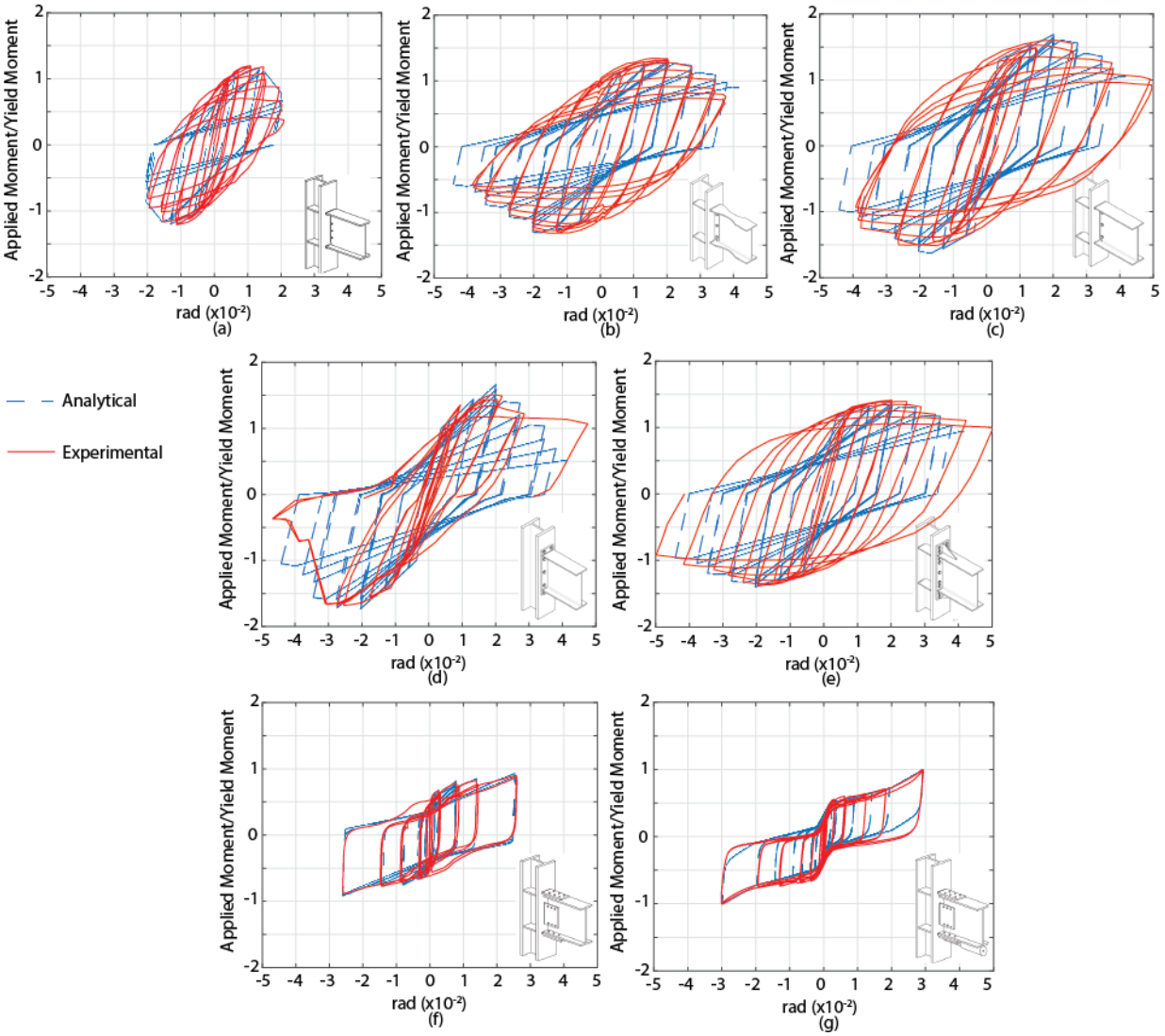


Figure 1: Comparison of experimental and analytical hysteretic behaviour for (a) PRENORTH, (b) RBS, (c) WUF, (d) WUEP, (e) WSEP, (f) SHJ and (g) SCSHJ

## 3 CALIBRATION OF ANALYTICAL MODELS

### 3.1 "Classic" connection models

The first five connections (Figure 1 (a), to (e)) were calibrated using variations of the Ibarra-Medina-Krawinkler material model (Ibarra et al. 2005). The IMK model was chosen as the default material because its parameters can be adjusted to capture many hysteretic characteristics, such as post-yield cyclic stiffness deterioration, yield strength degradation, in-cycle degradation and post-capping stiffness deterioration. The parameters of each analytical connection model were first calibrated using a multi-variable optimization framework based on a genetic algorithm, and then refined further by manual manipulations. Table 1 summarizes the most influential parameters of the IMK model used for each of these five connection types. Figure 2 shows the impact of these parameters on a generic moment-rotation hysteretic curve.

Table 1: Component test sections and major IMK parameters for pre-qualified connections

| Parameters | PRE-NORTH | RBS | WUF | WUEP | WSEP |
|---|---|---|---|---|---|
| Size of Test Beam/ Test Column | W920x201/ W360x382 (W36x135/ W14x257) | W920x201/ W360x382 (W36x135/ W14x257) | W610x101/ W360x179 (W24x68/ W14x120) | W610x101/ W360x179 (W24x68/ W14x120) | W920x223/ W360x634 (W36x150/ W14x426) |
| Analytical model used | Peak IMK | Peak IMK | Peak IMK | Pinch IMK | Peak IMK |
| Strain Hardening Ratio ($\alpha$) | 0.08 | 0.06 | 0.08 | 0.18 | 0.08 |
| Plastic Rotation ($\theta_p$) | 0.013 rad | 0.02 rad | 0.015 rad | 0.03 rad | 0.022 rad |
| Post-Capping Rotation ($\theta_{pc}$) | 0.02 rad | 0.2 rad | 0.2 rad | 0.4 rad | 0.5 rad |
| Ultimate Rotation ($\theta_u$) | 0.6 rad | 0.6 rad | 0.6 rad | 0.5 rad | 0.6 rad |
| Residual Strength Ratio ($M_r$) | 0.2 | 0.3 | 0.35 | 0.3 | 0.78 |
| Cyclic Deterioration Ratio ($D_r$) | 2.96 | 0.8 | 1.05 | 2.1 | 3.52 |

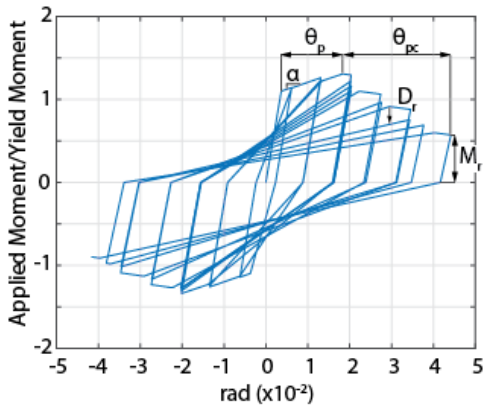


Figure 2: Generic moment-rotation with major IMK parameters

### 3.2 Sliding Hinge Joint (SHJ) model

The material model used for the sliding hinge joint consisted of a combination of the existing *Hysteretic* and the *Steel02* materials. Extensive documentation of each of these materials is available (Filippou et al. 1983). The two material models were combined using the *Parallel* material with equal weighting factors. Following this combination, a third uniaxial material model was added. This third material is the *Fatigue* uniaxial material model, allowing for the capturing of cyclic deterioration of the hysteretic parameters. This total combined material model is referred to as the *SHJ* material. The parameters of the first two material models control the behaviour of the *SHJ* material. A description of each of the parameters that modify this material is listed below, and calibrated values are provided in Figure 3 (a):

1. Stiffness (K): Initial stiffness
2. Activation Moment ($M_e$): Activation moment
3. 1st Post-Activation Stiffness Ratio ($\alpha_1$): Ratio of second stiffness to initial stiffness
4. Dependable Moment ($M_d$): Maximum moment for first post yield stiffness
5. 2nd Post-Activation Stiffness Ratio ($\alpha_2$): Ratio of third stiffness to initial stiffness

6. Yield Moment ($M_y$): Yield moment of beam
7. Pinching Displacement ($P_D$): Pinching factor for deformation during reloading
8. Pinching Force ($P_F$): Pinching factor for force during reloading
9. Curvature transition ($R_0$): Transition from initial to post activation stiffness assigned to *Steel02* material.
10. Isotropic Hardening Parameters ($a_1$, $a_3$): Change of strength after specific plastic strain assigned to *Steel02* material ($a_1$ for compression, $a_3$ for tension)
11. Isotropic Hardening Parameters ($a_2$, $a_4$): Activation of isotropic hardening parameter assigned to *Steel02* material (default = 1.0)

### 3.3 Self-Centering Sliding Hinge Joint (SCSHJ) model

The material model used for the self centering variant of the sliding hinge joint consisted of a combination of three existing material models that are already implemented in OpenSees. These existing material models were the *SelfCentering,* the *Steel02* and the *ElasticPPGap* materials al. 2008. The *Steel02* and *SelfCentering* materials control all the hysteretic behaviour between connection rotations of ±0.02 rad. Within these rotations, the model is controlled by defining the activation force (moment), the first and second dependable moments and the three stiffnesses between each point (initial, 1st post-activation and 2nd post-activation). At rotations larger than 0.02 rad, the *ElasticPPGap* material is used to modify the stiffness to the 3rd post-activation stiffness. The total combined material model is referred to as the *SCSHJpinch* material. The parameters of this material and their description are listed below and calibrated values are provided in Figure 3 (b):

1. Stiffness (K): Initial stiffness
2. Activation Moment ($M_e$): Activation moment
3. 1st Post-Activation Stiffness Ratio ($\alpha_1$): Ratio of second stiffness to initial stiffness
4. Dependable Moment ($M_d$): Maximum moment for first post yield stiffness
5. 2nd Post-Activation Stiffness Ratio ($\alpha_2$): Ratio of third stiffness to initial stiffness
6. Second Dependable Moment ($M_{d2}$): Maximum moment for second post yield stiffness
7. 3rd Post-Activation Stiffness Ratio ($\alpha_3$): Ratio of fourth and final stiffness to initial stiffness
8. Yield Moment ($M_y$): Yield moment of beam
9. Beta (β): Ratio of Forward to Reverse Activation Force for *SelfCentering* material
10. Curvature transition ($R_0$): Transition from initial to post activation stiffness assigned to *Steel02* material.
11. Lamda (λ): Ratio of stiffness defined by *SelfCentering* material to that defined by *Steel02* material
12. Theta (θ): Deformation at onset of final stiffness.

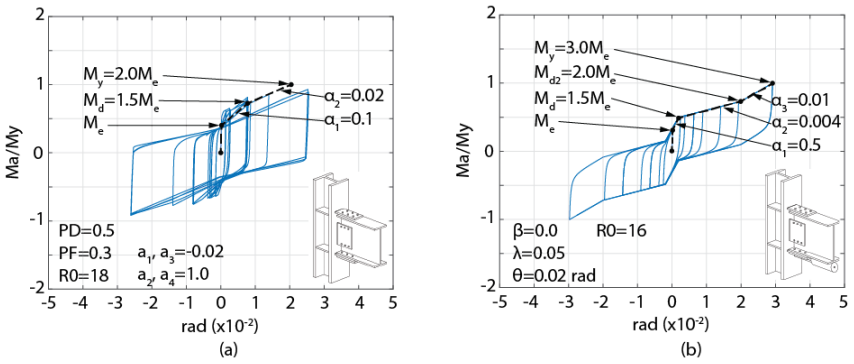


Figure 3: Parameters for (a) SHJ and (b) SCSHJ analytical models

## 4 VARIATION OF COLLAPSE PERFORMANCE DUE TO CONNECTION SELECTION

The collapse performance of a single archetype frame was computed using each of the seven MRF connection models. The archetype frame used for the collapse analysis was a six-storey frame located in Seattle, Washington on site class B. This frame was originally designed by Tsai and Popov (1988), before the Northridge earthquake, and was later redesigned with RBS connections by Hall (1995). Each of the six post-Northridge versions of the frame was verified to satisfy newer ASCE requirements (ASCE 2016). The selected frame is representative of one of two parallel perimeter frames in a structure with no irregularities. It has three bays of equal length and includes a taller bottom story that is susceptible to a soft storey failure mechanism (Hall 1995), as is common in west coast steel MRFs. All versions of this frame have a first-mode elastic period of 1.3 s. A leaning column was used to capture the second order P-$\Delta$ effects caused by the interior gravity frame. The six-storey frame model includes panel zone yielding using the Krawinkler spring box model (Gupta & Krawinkler 1999). Detailed information about the archetype frame can be found in Christopoulos & Filiatrault (2006).

The collapse analysis was conducted using a multiple stripe analysis (Baker 2015) with seven stripes selected at various multiples of the risk-targeted maximum considered earthquake ($MCE_R$) for the selected site per ASCE 7-16. The curve was fitted with log-normal collapse fragility curves using the maximum likelihood method described by Baker (2015). The $MCE_R$ spectral acceleration at the first-mode period for the archetype structure at this site was 0.44g. The chosen intensities for the stripes used for this analysis were 0.5x$MCE_R$, 0.75x$MCE_R$, 1.0x$MCE_R$, 1.25x$MCE_R$, 1.5x$MCE_R$, 2.0x$MCE_R$ and 3.0x$MCE_R$. Each stripe consisted of 40 components of ground motions taken from the NGA-West 2 Database (Chiou et al. 2008) and scaled using the conditional mean spectrum at the respective intensity (Baker & Lee 2017). Failure was defined as achieving any storey drift greater than 8%. Figure 4 shows the collapse fragility curves for all seven models.

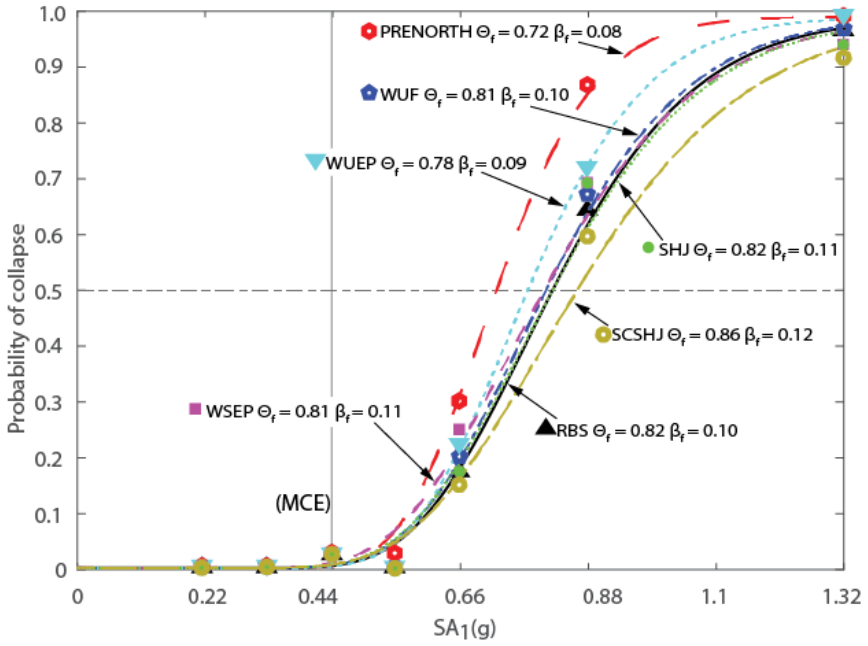


Figure 4: Collapse Fragility Curves for all seven frames

As was expected, the PRENORTH frame had the lowest median collapse capacity, at 0.72g. The largest median collapse capacity was achieved by the SCSHJ frame with a value of 0.86g. The 4 pre-qualified connections maintained similar median collapse capacities of 0.81g or 0.82g, with the exception of the WUEP frame, which had a somewhat lower value of 0.78g. This conclusion obtained from the comparison of the four prequalified connections was consistent with an earlier preliminary study (Steneker & Wiebe 2017). The frame using SHJ connections had nearly identical collapse performance when compared to the

RBS frame. However, as noted previously, the SHJ connection was designed with an activation force 45% lower than that of the beams yield moment. While this resulted in larger displacements, the energy dissipated by the SHJ connection was not a result of plastic hinging of the beam, but rather friction occurring between the sliding surfaces. Furthermore, the lower activation force of the SHJ connection limited the column and panel zone yielding during all of the ground motion events. When comparing the SHJ and SCSHJ frame, the addition of the self-centering ring springs resulted in an increase of 5% in median collapse capacity. This increase in performance was maintained at larger intensities of ground motions. The Beta values, which define the lognormal standard deviation of the log-normal fragility curves, remained constant at approximately 0.10 ($\pm$0.02). The uncertainty captured by this variable is limited to the record-to-record variability; other sources of uncertainties would also affect the collapse fragility curves for each of the frames.

## 5 SIGNIFICANCE OF BACKBONE VS RELOADING CURVE COMPONENTS

One limitation of using the Ibarra-Medina-Krawinkler (IMK) model when modelling the behaviour of MRF beam hinges is its restriction to piecewise linear loading and unloading stiffness values (Ibarra & Krawinkler (2005)). This limitation is observed when examining the major differences between the experimental and analytical moment rotation relationships in Figure 1 (a) to (e). While the IMK model is able to capture various post-yield phenomena and deterioration mechanisms relative to the backbone curve of the beam hysteretic behaviour, it is unable to capture the curved shape of the moment-rotation relationship in the reloading phase of the same hysteretic behaviour (in the second and fourth quadrants). These two regions are shown in Figure 5. Because this difference appears to be large, a sensitivity analysis was conducted in order to determine the impact of this hysteretic region on the collapse performance of the archetype frame considered.

The investigation was conducted using two IMK models calibrated for the same beam hinges with RBS connections. The first mois the aforementioned peak-oriented IMK hinge model, while the second is the bilinear IMK model. For comparison, the moment-rotation predictions of the peak oriented IMK model are superimposed on top of the component test results in Figure 6 (a), the bilinear IMK model is shown with the same experimental component test results in Figure 6 (b), and the two analytical IMK models are overlaid in Figure 6 (c). In contrast to the IMK peak-oriented model, the IMK bilinear model overestimates the reloading stiffness portion of the beam hinge hysteretic behaviour. However, since the bilinear IMK model uses the same 26 parameters as the peak-oriented model, the backbone curve portion of the behaviour can be calibrated in the same manner as the peak-oriented IMK model.

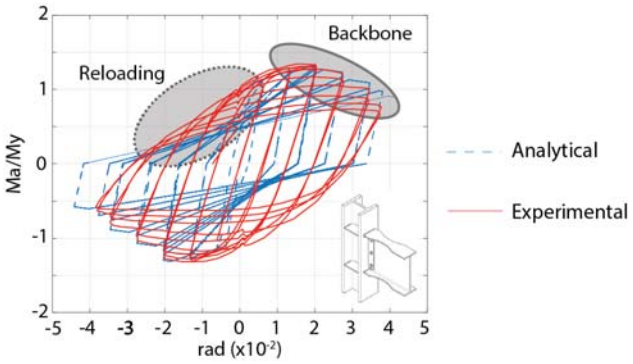


Figure 5: Location of backbone and reloading portions of hysteretic behaviour

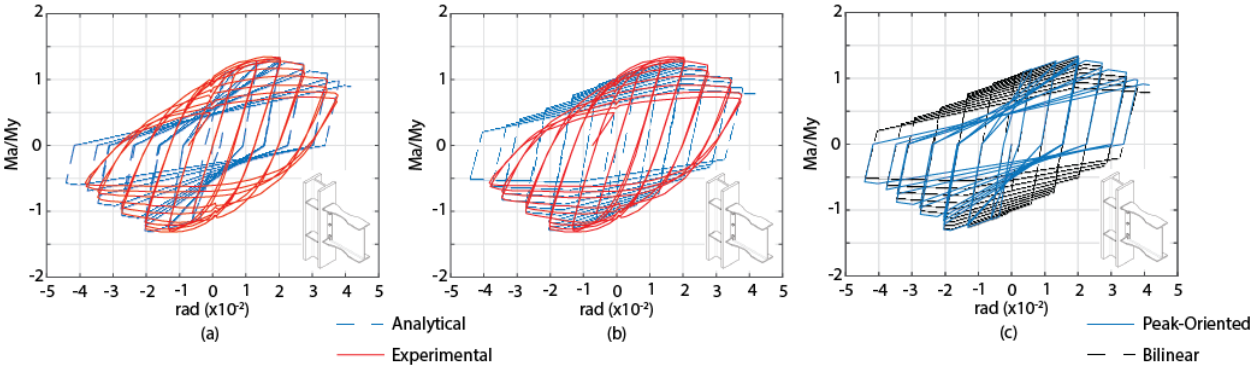


Figure 6: Comparison of hysteretic behaviour (a) Experimental and peak oriented IMK analytical model (b) Experimental and bilinear IMK analytical model (c) Peak oriented IMK and bilinear IMK model

Using the two models described above for the same archetype frame used throughout this study, two collapse analyses were conducted. The collapse fragility curves are shown in Figure 7, which shows nearly identical collapse performance. Only a single extra ground motion resulted in collapse of the frame at the 1.5xMCE$_R$ and 2.0xMCE$_R$ intensities using the peak-oriented IMK beam hinge model. Although this comparison is shown for only one of the five "classic" beam connections, the results suggest that the reloading stiffness portion of the beam hinge model is not as critical as the backbone model for this frame. However, this sensitivity analysis was limited in scope, and the characteristics of this frame, such as a soft storey or the use of RBS connections, may have an impact on this observation. Furthermore, the approximation of the inherent damping using the Rayleigh method based on the initial stiffness matrix may also have contributed to this minimal difference in collapse performance. While this method of modelling damping using the initial stiffness is commonly used, a frame modelled with tangent stiffness proportional Rayleigh damping may have different collapse behaviour due to the more frequent changes in stiffness during the reloading phase of the IMK model.

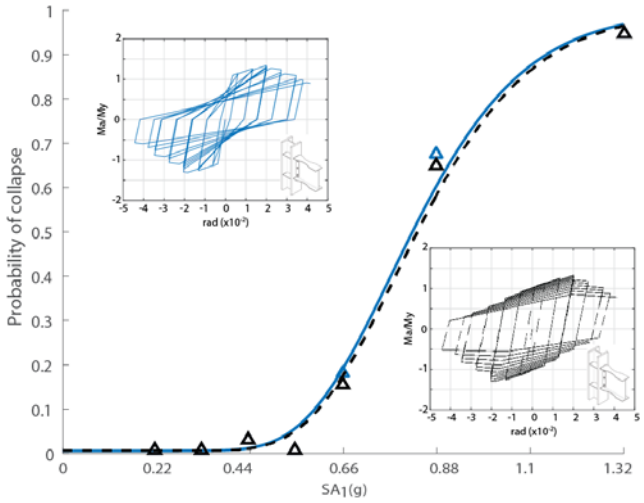


Figure 7: Comparison of collapse fragility curve for model using peak oriented IMK model (solid blue) and bilinear IMK model (dashed black)

## 6 CONCLUSION

This paper examined the hysteretic behaviour of seven steel moment resisting frame connections and their impacts on the overall frame performance. Specific hysteretic characteristics were summarized for seven different connection types: 1) a typical pre-Northridge connection, 2) a pre-qualified reduced beam section connection, 3) a pre-qualified welded unreinforced flange connection (WUEP), 4) a pre-qualified welded

unstiffened end plate connection, 5) a pre-qualified stiffened end plate connection, 6) a newly developed sliding hinge joint (SHJ) connection, and 7) a self-centering variant of the sliding hinge joint connection (SCSHJ). Analytical models calibrated in OpenSees were proposed for each of the seven connections, including newly developed models for both variants of the sliding hinge joint connection. The collapse performance of an archetype frame model incorporating each of the seven connection types was performed. While the WUEP connection had the lowest collapse performance, the variation among the four prequalified connections did not vary by more than 5%. The use of the SCSHJ connection in the place of SHJ connection resulted in a 5% increase in median collapse capacity. Finally, a short sensitivity analysis was conducted on the relative importance of capturing the reloading stiffness of the hysteretic behaviour of MRF connections. The numerical results indicate that the backbone portion of the hysteretic behaviour is more critical than the reloading stiffness values. Future work on the efficient implementation of these connections, and their influence on the global collapse performance of frame structures, as well as on residual displacements, is underway.

**Acknowledgements**

The authors would like to acknowledge the assistance of Dr. Charles Clifton, Dr. Greg MacRae and Dr. Hsen-Han Khoo for providing component test data for the SHJ and SCSHJ connections used in this paper. The authors would also like to acknowledge the National Science and Engineering Research Council (NSERC) for funding this research.

**References**

American Institute of Steel Construction. 2016. AISC 358-16: Prequalified Connections for Special and Intermediate Steel Moment Frames for Seismic Applications,

American Society of Civil Engineers. 2016. ASCE 7-16: Minimum Design Loads and Associated Criteria for Buildings and Other Structures,

Baker J., 2015. Efficient analytical fragility function fitting using dynamic structural analysis, *Earthquake Spectra.* **31** (1) 579-599

Baker J., Lee. C. 2017. An Improved Algorithm for Selecting Ground Motions to Match a Conditional Spectrum, *Journal of Earthquake Engineering,* (in Press), 1-16.

Bruneau M., Uang C.-M., & Sabelli R., 2011. Ductile Design of Steel Structure, second ed. McGraw Hill

Canadian Institute of Steel Construction. 2014. Moment Connections for Seismic Applications, 2nd Edition.

Chiou B., Darragh R., Gregor N. & Silva W. 2008. NGA Project Strong-Motion Database, *Earthquake Spectra.* **24** (1), 23-44

Choi, J., Stojadinovic, B., & Goel, S. 2002. Development of free flange moment connection. *University of Michigan, Department of Civil and Environmental Engineering, Ann Arbor.*

Christopoulos, C., and Filiatrault, A. 2006. “Principles of Supplemental Damping and Seismic Isolation,” IUSS Press, Istituto Universitario di Studi Superiori di Pavia, Pavia, Italy, 500 p.

Engelhardt M. D. & Sabol T. A. 1994. Testing of welded steel moment connections in response to the Northridge earthquake, *Northridge Steel Update Number 1*, AISC.

FEMA-350. 2000. Recommended Seismic Design Criteria for New Steel Moment-Frame Buildings.

Filippou, F. C., Popov, E. P., Bertero, V. V. 1983. Effects of Bond Deterioration on Hysteretic Behaviour of Reinforced Concrete Joints. *Report EERC 83-19, Earthquake Engineering Research Center, University of California, Berkeley.*

Gupta, A., & Krawinkler, H. 1999. Seismic Demands for Performance Evaluation of Steel Moment Resisting Frame Structures. *Stanford University, Department of Civil and Environmental Engineering, Stanford.*

Hall J. 1995. Parameter Study of the Response of Moment -Resisting Steel Frame Buildings to Near-Source Ground Motions. Sacramento, CA: *SAC95-05: Parametric Analytical Investigation of Ground Motion and Structural Response, Northridge Earthquake of January 17, 1994*.

Ibarra L. F., Medina R. A., & Krawinkler H. 2005. Hystertic models that incorporate strength and stiffness deterioration, *Earthquake Engineering and Structural Dynamics*, **34** (12): 1489-1511.

Ibarra L. F. & Krawinkler H. 2005. Global collapse of frame structures under seismic excitations, *Stanford Technical Report 152*

Khoo, H.H., Clifton, C., Butterworth, J. & MacRae, G. 2013. Experimental Study of Full-Scale Self-Centering Sliding Hinge Joint Connections with Friction Ring Springs, *Journal of Earthquake Engineering*. **17** (7): 972-997.

Lignos, D., & Al-Shawwa, N. 2010. Steel W-Shape Database. Web-Based Interactice Tools for Performance-Based Earthquake Eningeering: http://dimitrios-lignos.research.mcgill.ca/databases/index.php

McKenna F. & Scott M.H. 2000. Open system for earthquake engineering simulation, *University of California, Berkeley, CA*.

Popov E., Balan T., & Yang T.-S., 1998, Post-Northridge Earthquake Seismic Steel Moment Connections, *Earthquake Spectra*, **14** (4): 659-677.

Sumner, W., & Murray, T. 2002. Behavior of Extended End-Plate Moment Connections Subject to Cyclic Loading. *Journal of Structural Engineering*, **128**(4), 501-508.

Steneker, P. & Wiebe, L. 2017 Global Seismic Performance of Steel Moment Resisting Frames with Different Connection Details. *Proceedings of 16th World Conference on Earthquakes*, Paper Nº 3319

Tsai K.-C, & Popov E. 1988. Steel Beam-Column Joints in Seismic MRFs, Berkeley: *Earthquake Engineering Research Center, University of California*